# Ovarian germline stem cell dedifferentiation is cytoneme-dependent

Catherine Sutcliffe[1], Nabarun Nandy[1], Hilary L. Ashe[1,*] and Scott G. Wilcockson[1,2,*]

[1]Faculty of Biology, Medicine and Health, University of Manchester, Manchester M13 9PT, UK.

[2]Present address: Developmental Signalling Laboratory, The Francis Crick Institute, London NW1 1AT, UK.

*Correspondence: hilary.ashe@manchester.ac.uk, scott.wilcockson@crick.ac.uk

## Abstract

Progenitor cell dedifferentiation is important for stem cell maintenance during tissue repair and age-related stem cell decline. Here, we use *Drosophila* ovarian germ cells as a model to study the role of cytonemes in BMP signalling-directed dedifferentiation to germline stem cells. We provide evidence that differentiating germ cell cysts extend cytonemes towards the niche during dedifferentiation to reactivate BMP signalling. We show that the Enabled (Ena) actin polymerase is localised to the tips of germ cell cytonemes and is necessary for robust cytoneme formation, as its mislocalisation reduces the frequency, length and directionality of cytonemes. Furthermore, specifically perturbing cytoneme function through Ena mislocalisation reduces germ cell BMP responsiveness and the ability of differentiating cysts to dedifferentiate. We discuss how cytonemes may be widely used by differentiating cells to re-establish niche contact and signal responsiveness following stem cell loss, promoting robust dedifferentiation of stem cells in diverse contexts.

## Introduction

The germline stem cell (GSC) niche is composed of specialised somatic cells, including cap cells (CpCs) and escort cells (ECs), which provide self-renewal signals to support 2-3 GSCs per germarium (Xie and Spradling 2000; Kirilly and Xie 2007). GSCs undergo asymmetric division to form one GSC, which remains in the niche, and one daughter cystoblast (CB) which leaves the niche and undergoes differentiation. The key signal promoting stem cell identity is Bone Morphogenic Protein (BMP) signalling, driven primarily through the ligands Decapentaplegic (Dpp) and Glass Bottom Boat (Gbb), resulting in phosphorylation of the transcription factor Mad (Xie and Spradling 1998; Song et al. 2004). In addition, GSCs are anchored to the CpCs through E-Cadherin (Ecad) mediated cell adhesion at adherens junctions. (Song et al. 2002). GSCs are therefore identifiable by their anterior localisation, high pMad levels, and the presence of the spectrosome, a germline-specific Spectrin-rich endomembrane organelle that becomes a branched structure (fusome) in more developed cysts (Figure 1A). BMP signalling silences the transcription of the differentiation master gene, *bag of marbles* (*bam*) (Chen and McKearin 2003; Song et al. 2004). Upon GSC division, the daughter cell that exits the niche has reduced pMad and upregulates *bam* expression, triggering germline differentiation to a CB (McKearin and Spradling 1990; McKearin and Ohlstein 1995). A single CB undergoes four rounds of mitosis with incomplete cytokinesis to form 2-, 4-, 8- and 16-cell cysts (cc) with interconnected fusomes (Lin et al. 1994; de Cuevas and Spradling 1998).

Restricted access to BMP is an important regulatory step that limits stem cell identity to those cells in direct contact with the niche. GSC-niche signalling is mediated in part by cytonemes, actin-based extensions which project toward and from signalling centres (Ramirez-Weber and Kornberg 1999). It has been shown that early germ cells (GCs) form actin-rich projections and GSCs extend cytonemes to probe the niche and access Dally-bound Dpp to promote BMP signal transduction. Dpp signalling induces the formation of more stable microtubule enriched cytosensors, which also receive the BMP signal but provide feedback inhibition through signal suppression (Wilcockson and Ashe 2019). Short cytonemes mediating Hedgehog (Hh) distribution have also been detected in the germline niche emanating from Hh-producing CpCs toward receiving ECs (Rojas-Rios et al. 2012). Thus, cytonemes play an integral role in cell communication in the ovarian germline.

Many factors, particularly those associated with the actin cytoskeleton, have been identified as regulators of cytoneme formation (Daly et al. 2022). Enabled (Ena), an actin polymerase, is associated with filopodia extension in many cellular contexts (Bear et al. 2002; Lebrand et al. 2004; Mejillano et al. 2004; Barzik et al. 2005). Ena localises to the tips of lamellipodia and filopodia (Rottner et al. 1999; Bear et al. 2000; Bear et al. 2002; Svitkina et al. 2003), where it recruits Profilin/actin complexes to enhance F-actin polymerization (Kang et al. 1997; Pasic et al. 2008) and filopodia formation (Schirenbeck et al. 2006; Applewhite et al. 2007). In addition, Ena localises to focal adhesions (Reinhard et al. 1995; Gertler et al. 1996) and adherens junctions (Scott et al. 2006). In the latter, Ena plays a role in Ecad localisation (Sano et al. 2012) and in cytoskeletal regulation at Ecad contact sites (Scott et al. 2006). Ena is therefore an attractive candidate that could regulate GSC cytoneme formation and niche interaction.

It has previously been shown that transient induction of *bam* expression using a heatshock (HS)-inducible transgene, *hs-bam*, causes complete loss of GSCs from the niche through Bam-induced differentiation within 24 hrs (Ohlstein and McKearin 1997). Following this, over the course of a few days, GCs can recolonise the niche and fully recover GSC loss. This is driven by cyst dedifferentiation, resulting in gradual cyst breakdown to form single cells (Kai and Spradling 2004). Here, we used this system to test the role of cytonemes in mediating BMP-dependent dedifferentiation. We show that Ena regulates GC cytoneme formation and its loss-of-function reduces the robustness of cytoneme formation. Disrupting cytoneme formation significantly reduces GC responsiveness to BMP signalling and thus precludes GC dedifferentiation and niche recolonisation.

## Results

### Early cysts can dedifferentiate to recolonise an empty GSC niche

To investigate a role for cytonemes in GSC dedifferentiation, we first established the timeline of BMP responsiveness and dedifferentiation using a previously described assay (Kai and Spradling 2003; Kai and Spradling 2004). We transiently induced expression of the differentiation factor *bam* throughout the germarium using a *hs-bam* transgene. The number of pMad positive early GCs was visualised in the days post-HS (dpHS) to quantify the level of dedifferentiation and recovery of niche-associated GSCs. The presence of pMad indicates that the cells are responding to niche derived Dpp signalling. A transgene with the *bam* promoter driving GFP (Chen and McKearin 2003) was also used to mark Bam positive differentiating cells. Pre-HS, pMad positive GSCs can be identified by the presence of an anteriorly localised spectrosome (visualised by αSpectrin staining) associated with niche CpCs (Figure 1A, B). GFP is detected in differentiating CBs and developing cysts located more posteriorly (Figure 1B).

One dpHS, pMad and spectrosome positive GSCs are absent and GFP can be detected in the cells directly adjacent to the niche with branched fusomes (Figure 1C, H). This indicates that GSCs and early CBs have been lost due to differentiation (Figure 1A). Indeed, almost all germaria contain pMad-negative cysts (Figure 1H; 1 dpHS cf day 0 pre-HS). At 3 dpHS, while ~60% of germaria still only contain differentiated cells (Figure D), ~40% now contain pMad-positive and GFP-negative cells adjacent to the niche, consistent with dedifferentiation (Figure 1E). The pMad accumulation is either associated with a spectrosome-containing GSC in direct contact with the niche, or a cyst containing a branched fusome (Figure 1H). Within these pMad positive cysts (typically at the 4cc stage) only the cells which are in direct contact with the CpCs, the source of secreted Dpp, are pMad positive (Figure 1I, J). Fusome thinning and scission, which are associated with cyst breakdown during dedifferentiation (Kai and Spradling 2004), are also evident at the 4 cc stage.

By 6 dpHS, the majority of germaria continue to display a lack of dedifferentiation such that all early GCs are lost, and only later stage cysts are present (Figure 1F, H). This suggests that after 3 dpHS there is no further dedifferentiation of cysts. However, in germaria where dedifferentiation has occurred, pMad- and spectrosome-positive GSCs are detected in the niche (Figure 1G). The proportion of germaria with pMad-positive GSCs that have dedifferentiated is highest at 6 dpHS (Figure 1H). Together, these data show that this post-HS time course allows us to capture different events during GC dedifferentiation, including the ability of cysts to respond to Dpp signalling, followed by cyst breakdown, and the recolonisation of the germline stem cell niche.

### Dedifferentiating GCs extend cytonemes during niche recolonisation

As we previously showed that actin- and tubulin-based cytonemes enable GSCs to access niche Dpp (Wilcockson and Ashe 2019), we used the dedifferentiation assay to test whether cytonemes play a role in the dedifferentiation of early cysts by enabling access to niche derived Dpp. To visualise cytonemes during dedifferentiation, we used a *LifeAct-GFP* reporter driven by *nosGAL4VP16* in GCs 3 and 4 dpHS. Pre-HS control germaria were also studied, which contain GSCs with niche directed cytonemes (Figure 2A).

Post-HS, germaria in various stages of dedifferentiation were identified. Some germaria have only early or late cysts remaining and lack cytonemes (Figure S1A, B). In contrast, other germaria show pMad-negative early cyst cells extending cytonemes toward the niche (Figure 2B, S1D). In some germaria with cysts, extra somatic cells are found to accumulate in the niche (Figure 2B, S1A, B), some of which are pMad-positive indicating that they are receiving BMP signalling. This is consistent with a previous report of somatic escort cells and follicle cell progenitors populating the niche after GSC loss following *hs-bam* expression (Kai and Spradling 2003). We speculate that accumulation of non-germline cells in the niche can block access for the differentiating cysts preventing them from reoccupying the niche (see Discussion).

We also observed germaria containing cysts with low level pMad and short, niche-directed cytonemes (Figure S1C), as well as germaria in which GSCs have recolonised the niche (Figure 2C, S1E). These pMad-positive GSCs have cytonemes probing the niche (Figure 2C, S1E), as observed for non-HS controls (Figure 2A). Together, these data suggest that post-HS, when the niche is empty, the cysts begin to extend cytonemes toward the niche. Over time, if the cysts are not blocked by the accumulation of somatic cells in the niche, they are able to access Dpp, reactivate pMad and dedifferentiate as GSCs (Figure 2D).

## Ena is localised at the tips of GSC and CB cytonemes

To test whether cytonemes promote GSC-niche recolonisation by allowing access to niche Dpp, we sought to disrupt GC cytonemes without affecting other critical actin functions. To this end, we explored Ena as a potential cytoneme regulator, because it regulates filopodia emergence, without affecting cell division (Bear et al. 2002; Gates et al. 2007). We initially visualised Ena localisation in GCs. Using antibody staining we identified Ena in early GCs and at the interface between the CpCs and the GSCs (Figure 3A). Using Vasa staining to mark GCs, Ena was also identified at the tips of GSC cytonemes oriented towards the niche (Figure 3Bi, ii), consistent with its role as an actin polymerase (Breitsprecher et al. 2008; Winkelman et al. 2014). We also detected Ena at the tips of CB cytonemes (Figure 3C) and lamellipodia-like projections (Figure 3Ci, bracket), suggesting that Ena may be a general regulator of GC cytonemes.

Ena can also play a role in cellular adhesion and we observe Ena concentrating at both GSC-CpC and CpC-CpC tricellular junctions (Figure 3D, E). However, we do not observe Ena at the GSC-niche interface with Ecad. We further characterised Ena localisation in GCs by specifically expressing an *ena-GFP* transgene in the germline using the *nosGAL4VP16* driver. GSC derived Ena-GFP also localises to cytoneme tips and to a lesser extent along the cytoneme length (Figure S2A). The slightly less restricted Ena-GFP localisation, compared to that observed with the Ena antibody, may reflect some Ena-GFP aggregation resulting from its overexpression. Overall, this localisation suggests that Ena may be important for cytoneme extension and, therefore, a potential selective target for manipulating cytoneme behaviour.

To disrupt Ena function specifically in the ovarian germline, we used an established Ena mislocalisation construct, *FP4mito.* FP4mito contains a multimerised FPPPP (FP4) motif, which is bound by the N-terminal EVH1 domain of Ena with high affinity (Niebuhr et al. 1997), fused to a mitochondrial outer membrane targeting signal. As targeting the FP4 motif to mitochondria mislocalises Ena there, expression of a *FP4mito* transgene *in vivo* inhibits Ena function (Gates et al. 2007; Gates et al. 2009; Homem and Peifer 2009; Nowotarski et al. 2014). To specifically mislocalise Ena in GCs, *FP4mito* was expressed in the germline using *nosGAL4VP16* alone or with *LifeAct-GFP* to visualise F-actin. Both Ena (Figure S2B) and F-actin (Figure S2D) are observed to accumulate in cytoplasmic aggregates, only GCs, in *FP4mito* expressing germaria, as described previously for *FP4mito* expressing epidermal cells in the *Drosophila* embryo (Gates et al. 2007). The Ena-GFP reporter was also observed to be mislocalised in the *FP4mito* background (Figure S2C). However, we observe no effect on Ecad levels (Figure 3F, G), suggesting that Ena mislocalisation does not impact GSC-niche adhesion at homeostasis. These data show that FP4mito efficiently mislocalises Ena in the ovarian germline and therefore provides a potential tool for the perturbation of cytoneme formation.

### Ena regulates GC cytoneme formation

Next, we tested the impact of FP4mito on cytoneme formation by quantifying the length of GSC and CB cytonemes labelled with LifeAct-GFP (Figure 4Ai, ii). We found that when Ena is mislocalised to mitochondria, the mean GSC cytoneme length is significantly reduced by ~2-fold (Figure 4B). This is consistent with previous studies where mislocalisation of Ena with *FP4mito* results in a reduced length of filopodia in leading edge cells during *Drosophila* dorsal closure (Gates et al. 2007).

We next imaged LifeAct-GFP live in germaria cultured *ex vivo* (Figure 4C) and quantified the number of cytonemes on the GSCs and CBs of control and *FP4mito* expressing germaria. We observed significantly fewer cytonemes on both the GSCs (Figure 4D) and CBs (Figure 4E) of *FP4mito* germaria compared with controls. We then characterised the directionality of GSC cytonemes. Briefly, a line was drawn from the centre of each GSC toward the niche. Cytonemes within a 45° angle from this line were counted as being anteriorly localised, while cytonemes oriented more than 45° were assigned as lateral (Wilcockson and Ashe 2019). *FP4mito*-expressing GSCs display a significant shift from anteriorly localised to more lateral cytonemes than controls (Figure 4F), indicating that the directionality of cytoneme formation is perturbed. In conclusion, Ena mislocalisation perturbs GC cytoneme formation and those that are formed are shorter and misoriented relative to the niche.

## Ena mislocalisation impairs BMP signal reception and stem cell fitness

As cytonemes enable GSCs to access niche sequestered Dpp, we tested the effect of perturbing cytoneme formation on BMP signalling and stem cell self-renewal by quantifying the number of pMad-positive GCs in the *FP4mito* expressing background. Wildtype germaria typically contain 3-4 pMad positive GCs, i.e. GSCs and CBs, whereas two or less indicates aberrant differentiation and 5 or more indicates delayed differentiation[12]. By 1-week post-eclosion, there is a small increase in the number of pMad positive GCs lost to differentiation in *FP4mito* germaria compared to controls (Figure 5A, B). Furthermore, *FP4mito* expressing GSCs display significantly reduced pMad levels (Figure 5A, C), consistent with reduced Dpp signal reception when cytonemes are disrupted. By 2.5 weeks post-eclosion, we observe an increase in the percentage of *FP4mito* germaria exhibiting aberrant differentiation, compared to control germaria (Figure 5D, E). Together, these data show that mislocalisation of Ena perturbs cytoneme formation and the ability of GSCs to respond to niche BMP signalling, resulting in ageing associated decline in the stem cell pool.

## Ena mislocalisation impairs GC dedifferentiation

Given that perturbation of cytoneme formation disrupts BMP signal reception, we next used FP4mito to test whether cytonemes are necessary for GC dedifferentiation. Specifically, we transiently induced the *hs-bam* transgene as before (Figure 1A), in either a *nosGAL4VP16>FP4mito* or *nosGAL4VP16* control background. We performed a pair-wise comparison of the number of germaria with pMad positive GCs (i.e. GSCs or CBs) 1 vs 6 dpHS. On day 1 in both conditions, the majority of GCs are pMad negative and have branched fusomes (Figure 6A, D, G, H).

On day 6, a proportion of control *nosGAL4VP16* germaria contain pMad positive GSCs and a round spectrosome, consistent with niche recolonisation (Figure 6B, C). Germaria lacking pMad positive cells and round fusomes were also observed, indicative of a lack of germline recovery such that all GCs were lost due to differentiation. Quantitation of these data show that ~40% of control germaria have a significant recovery of pMad positive GCs (Figure 6G), consistent with the data presented in Figure 1.

*FP4mito* germaria with either pMad-negative (Figure 6E) or pMad-positive GCs (Figure 6F) were also observed 6 dpHS. However, in contrast to control germaria, there is little or no recovery of pMad positive GSCs in *FP4mito* expressing germaria (Figure 6H, cf 6G). Additionally control germaria have higher numbers of pMad positive GSCs compared to *FP4mito* germaria (Figure 6I), indicating that the *FP4mito* GCs are less able to respond to Dpp signalling. Together, these results indicate that FP4mito, which causes Ena mislocalization and subsequent cytoneme dysfunction, prevents cyst dedifferentiation. These data are consistent with cytonemes playing an important role in the ability of cysts to respond to the self-renewal Dpp signal which is necessary for GCs can recolonise an empty niche.

## Discussion

Here, we provide evidence that actin-rich cytonemes, which are present on all early ovarian GCs (Wilcockson and Ashe 2019), are both necessary at homeostasis for robust BMP signal activation and to promote dedifferentiation of cysts to GSCs. Our data support a necessity for cytonemes in promoting stem cell fitness and the prevention of ageing-associated decline in the stem cell pool. Furthermore, cytonemes mediate niche contact and responsiveness to the BMP self-renewal signal during recolonisation of the niche (Figure 7). As we only detect cytonemes up to the 8cc stage (Figure 2B, S1A), this may explain why dedifferentiation of 16cc does not occur. Recently, the changes in the transcriptome and translatome during GSC differentiation have been described, and this has revealed two major waves of changes separated by an inflection point around the 4cc stage. From the 8cc stage onwards, gene expression changes associated with terminal differentiation occur (Samuels et al. 2024). This transition is also linked to dramatic changes in actin dynamics. Waves of contractile cortical actin are suppressed in 4-8cc and initiate in 16cc to promote their encapsulation by follicle cells prior to oocyte maturation (Chanet and Huynh 2020). It is possible that the gene expression and proteome changes that occur in the 8cc prevent the cells from forming cytonemes, further committing the cells to terminal differentiation.

We find that only a proportion of cysts are capable of dedifferentiation. We observed additional somatic cells colonising the niche, consistent with a report of escort cells initially entering the empty niche and responding to Dpp (Kai and Spradling 2003). A minority of escort cells express low levels of Dpp, which can increase the efficiency of dedifferentiation (Liu et al. 2015). However, *dpp* transcription in the escort cells was found to be stochastic, both spatially and temporally, and only detectable in around one quarter of germaria (Liu et al. 2015). Based on these observations, it is likely that many of the escort cells that have entered the empty niche following *hs-bam*-induced differentiation do not express *dpp*. Therefore, we suggest that the escort cells colonising the niche can both form a barrier to GSC-niche contact and outcompete the differentiated cysts for Dpp.

Our data show that Ena loss-of-function could be a useful tool for dysregulating cytoneme function in different contexts. Ena is localized to cytoneme tips, as observed in the filopodia of leading-edge cells during dorsal closure (Homem and Peifer 2009).

Using a *FP4mito* transgene to mislocalise Ena resulted in less frequent and shorter cytonemes, again consistent with the effects of Ena mislocalization on filopodia (Gates et al. 2007; Homem and Peifer 2009). While there are contexts where *FP4mito* expression phenocopies *ena* loss-of-function mutants (Gates et al. 2007; Gates et al. 2009), there are also examples where a stronger or different phenotype is observed with *FP4mito* compared to *ena* mutants (Gates et al. 2009; Homem and Peifer 2009). This is likely because a subset of cellular Diaphanous (Dia), a processive actin polymerase, can be mislocalised to mitochondria with Ena upon expression of *FP4mito* (Homem and Peifer 2009; Nowotarski et al. 2014). Indeed, loss of Dia disrupts cytoneme formation in ovarian GSCs and other contexts[12,44-46] and both Ena and Dia also have roles in mediating adhesion, with Dia having a role in Ecad endocytosis in epithelial cells[47] and GSCs[12]. Bam promotes GC differentiation by the post-transcriptional down-regulation of Ecad[48,49] which must be re-expressed during dedifferentiation. Therefore, it is possible that disruption to adhesion could impact dedifferentiation by precluding the formation of stable GC-niche interactions. However, *FP4mito* expression does not appear to affect GSC-niche Ecad levels at homeostasis suggesting that Dia function is largely unaffected. Indeed, our data show that targeted Ena loss-of-function could be a useful tool for dysregulating cytoneme function in different contexts.

Dedifferentiation is critical to repair tissue damage (Guo et al. 2022) and underpins the regenerative medicine strategies that rely on cellular reprogramming to induced pluripotent stem cells (Takahashi and Yamanaka 2016). In Dictyostelium, dedifferentiation occurs largely through a reversal of the gene expression programme and is robust to genetic perturbation (Nichols et al. 2020). We speculate that cytonemes will promote robust signalling responses during dedifferentiation in different contexts.

Another example where cytonemes may promote dedifferentiation is in spermatogonial cysts in the *Drosophila* testis. Following transient *hs-bam* expression, around half of the dedifferentiating 4-cell cysts had actin-based protrusions compared with only around 8% of control cysts (Sheng et al. 2009). Dedifferentiation is also associated with disease, for example neuronal dedifferentiation in early-onset familial Alzheimer's disease (Caldwell et al. 2020) or epithelial dedifferentiation to cancer stem cells to sustain tumour growth (Schwitalla et al. 2013). As cytoneme-mediated communication between cancer and non-cancer cells has been described (Rogers et al. 2023), cytonemes may also be a useful target for diseases caused by cellular dedifferentiation.

## Materials and Methods

### Fly Stocks

All experimental crosses were undertaken at 25°C on standard fly media (yeast 50g/L, glucose 78g/L, maize 72g/L, agar 8g/L, 10% (v/v) nipagin in ethanol 27ml/L and propionic acid 3ml/L). Stocks used are listed in Table 1.

**Table 1**

| | | |
|---|---|---|
| *D. melanogaster; y[1] w[67c23]* | Bloomington | Cat#6599; RRID:BDSC_6599 |
| *D. melanogaster*; *w*∗; GAL4::VP16-nos* | Bloomington | Cat#4937; RRID: BDSC_4937 |
| *D. melanogaster; M{w[+mC]=UASp-LifeAct.mGFP6}ZH-2A, w[∗]* | Bloomington | Cat#58717; RRID: BDSC_58717 |
| *D. melanogaster; w[*]; M{w[+mC]=UASp-Lifeact.TagRFP.H}ZH-51D/CyO* | Bloomington | Cat#58717; RRID: BDSC_58717 |
| *D. melanogaster;* w[1118]; P{w[+mC]=hs-bam.O}11d/TM3, Sb[1] | Bloomington | Cat#24637; RRID:BDSC_24637 |

| | | |
|---|---|---|
| *D. melanogaster;* P{w[+mC]=hs-bam.O}18d, w[1118] | Bloomington | Cat#24636; RRID:BDSC_24636 |
| *D. melanogaster; y[1] w[*]; P{w[+mC]=UAS-FLAG-HA-FP4mito}3* | Bloomington | Cat#58481; RRID:BDSC_58481 |
| *D. melanogaster; w*;P{w[+mC]=UASp-halo7-FP4mito}attP40* | This study | |
| *D. melanogaster; w∗;*<br>*bam-GFP* | (Chen and McKearin 2003) | Chen and Mc Kearin 2003 |
| *D. melanogaster; w[*]; P{w[+mC]=Ubi-GFP.ena}3* | Bloomington | Cat#28798; RRID:BDSC_28798 |
| *D. melanogaster; y w M(eGFP, vas-int, dmRFP)ZH-2A; P{CaryP}attP40* | University of Cambridge | Stock 13-20 |

**Transgenic line generation**

To generate *pUASp-FP4mito-Halo7-attB, actin A* was amplified from genomic DNA from the line *y[1] w[*]; P{w[+mC]=UAS-FLAG-HA-FP4mito}3* (Bloomington Cat#58481; RRID:BDSC_58481) and *Halo7* was amplified from *UAS-7xHalo7::CAAX* (Addgene # 87647) (Sutcliffe et al. 2017) using the below primers and inserted into *pUASP-attB* (DGRC Stock 1358; RRID:DGRC_1358) digested with XbaI and KpnI.

ActA F: CGGGGATCAGATCCGCGGCCGCCAAAATGGCAGAAATCGGTACTGGC

ActA R: TGAGTCCGGAACTAGTCTCGAGACTAGTAGATCTG

Halo7 F: CGAGACTAGTTCCGGACTCAGATCTATCGTAGCT

Halo7 R: ACGTTCGAGGTCGACTCTAGAAGCTAGCCTAGGCTCGAGA

*pUASp-FP4mito-Halo7-attB* was microinjected into *y w M(eGFP, vas-int, dmRFP)ZH-2A; P{CaryP}attP40* (Stock 13-20 The University of Cambridge Fly Facility) using *phiC31* mediated transgenesis at the University of Manchester fly facility.

### Heat shock

Flies one and two days post eclosion were heat shocked in vials containing a circle of Whatman paper to absorb condensation. Heat shocks were performed in a waterbath at 37°C. Vials were heat shocked for 1 hour 30 minutes at 37°C and then returned to 25°C for 1 hour before a second 1 hour 30 minute heat shock at 37°C. After the two heat shocks, flies were transferred to a new vial and returned to 25°C for aging.

### Immunofluorescence

For standard antibody stain ovaries were dissected in 1xPBS and fixed in 4% formaldehyde for 20 minutes at room temperature. Ovaries were blocked in 5x Western Blocking buffer (Merck 11921673001) or 10% BSA in 1xPBST (0.1% Tween 20) for 1 hour and then incubated with primary antibody at 4°C overnight. Antibody concentrations used were 1:500 anti-pMad and 1:50 anti-Spectrin, 1:50 anti-Ena, 1:500 anti-GFP, 1:500 anti-Vasa. Secondary antibodies were used at 1:1000. Antibody sources are shown in Table 2.

### Cytoneme Staining

For antibody staining of cytonemes, ovaries were dissected in PEM buffer (80mM PIPES, 5mM EDTA, 1mM Magnesium chloride, pH7.4 adjusted with NaOH) and fixed immediately in PEM with 4% formaldehyde, 5μM paclitaxel, 1μM calcium chloride for 30 minutes at room temperature. Washes were carried out in 1xPBST, 0.1% Tergitol (15-s-9). Ovaries were blocked in 5x Western Blocking buffer (WB) for 1 hour and then incubated overnight at 4°C in 1x WB with primary antibody. Antibody concentrations used were 1:250 anti-pMad, 1:250 anti-GFP, 1:25 anti-DCAD.2, 1:250 anti-tdTomato, 1:25 anti-Spectrin and 1:25 anti-Ena. Antibody sources are shown in Table 2. Ovaries were washed in 1xPBT and then incubated at room temperature for 2 hours in 0.1x WB with secondary antibody at 1:1000. Ovaries were washed in 1xPBT four times, including a wash containing DAPI (1µg/ml). Phalloidin staining was carried out in the penultimate wash (0.033µM in 1xPBST) for 30 minutes at room temperature. Ovaries were mounted in Prolong Diamond or Prolong Gold.

**Table 2**

| | | |
|---|---|---|
| Anti-GFP | Abcam | Cat#Ab6673<br>RRID:AB_305643 |
| Anti-pSmad3 Phospho (pS423/425) [EP823Y] | Abcam | Cat Ab52903<br>RRID:AB_765068 |
| Anti-Spectin 3A9 (323 or M10-2) | Hybridoma Bank | AB_528473<br>RRID:AB_528473 |
| Anti-Enabled 5G2 | Hybridoma Bank | AB_528220<br>RRID:AB_528220 |
| Anti-DCAD2 | Hybridoma Bank | AB_528120<br>RRID:AB_528120 |
| Anti-Vasa (d-260) | Santa Cruz (discontinued) | Cat# sc-30210<br>RRID:AB_793874 |
| Anti-Cytochrome C (33-8200) | Invitrogen | Cat# 33-8200<br>RRID:AB_2533141 |
| Donkey anti-Rabbit IgG (H+L) Highly Cross-Adsorbed Secondary Antibody, Alexa Fluor™ 647 | Thermo Fisher Scientific | Cat# A-31573<br>RRID:AB_2536183 |
| Donkey anti-Goat IgG (H+L) Cross-Adsorbed Secondary Antibody, Alexa Fluor™ 488 | Thermo Fisher Scientific | Cat# A-11055<br>RRID:AB_2534102 |
| Donkey anti-Rat IgG (H+L) Highly Cross-Adsorbed Secondary Antibody, Alexa Fluor™ 647 | Thermo Fisher Scientific | Cat# A78947,<br>RRID:AB_2910635 |
| Donkey anti-Rat IgG (H+L) Highly Cross-Adsorbed Secondary Antibody, Alexa Fluor™ 594 | Thermo Fisher Scientific | Cat# A-21209,<br>RRID:AB_2535795 |

| | | |
|---|---|---|
| Donkey anti-Rabbit IgG (H+L) Highly Cross-Adsorbed Secondary Antibody, Alexa Fluor™ 594 | Thermo Fisher Scientific | Cat# A-21207, RRID:AB_141637 |
| Donkey anti-Mouse IgG (H+L) Highly Cross-Adsorbed Secondary Antibody, Alexa Fluor™ 594 | Thermo Fisher Scientific | Cat# A-21203, RRID:AB_2535789 |
| Donkey anti-Mouse IgG (H+L) Highly Cross-Adsorbed Secondary Antibody, Alexa Fluor™ 555 | Thermo Fisher Scientific | Cat# A-31570, RRID:AB_2536180 |
| Donkey anti-Rabbit IgG (H+L) Highly Cross-Adsorbed Secondary Antibody, Alexa Fluor™ 488 | Thermo Fisher Scientific | Cat# A-21206, RRID:AB_2535792 |

## Live imaging

Live imaging was performed as described (Wilcockson and Ashe 2021).

## Imaging Settings

Imaging was performed on a Leica SP8 inverted microscope with either a HC PL APO CS2 40x/1.30 oil immersion objective or HC PL APO CS2 motCORR (Water) immersion objective or a Zeiss 980 Axio Observer.Z1 / 7 with a Plan-Apochromat 63x/1.40 Oil DIC M27 objective.

## Quantification of cytonemes

Cytoneme length was measured on Image J from the base to the tip of using the measure function as described (Wilcockson and Ashe 2019).

### pMad intensity Quantification

pMad intensity was measured by taking the Integrated Density (IntDen) of the pMad positive cell on Image J using the measure plugin. It was background corrected and normalised to the DAPI stain within the same area, as indicated below. 32 GSCs were analysed per genotype.

Normalised pMad Intensity = pMad IntDen – (Area x Mean background)/ DAPI IntDen

### Ecad intensity Quantification

Ecad intensity was measured on Image J using the measure plugin and plotted on GraphPad Prism (RRID:SCR_002798).

### Statistical Tests

Images were processed using Fiji (Schindelin et al. 2012). Graphs were plotted and analysis was performed on GraphPad Prism (RRID:SCR_002798).

### Competing interest statement

The authors declare no competing interests.

### Acknowledgements

We thank Tom Millard for suggesting Ena as a target, and Sanjai Patel, the University of Manchester Fly Facility and Bioimaging Facility for support. This work was supported by a Biotechnology and Biological Sciences Research Council project grant (BB/V015060/1) to H.L.A.

## Author contributions

Conceptualisation: C.S., H.L.A., S.G.W.; Investigation: C.S., N.N., S.G.W.; Formal Analysis: C.S., N.N., S.G.W.; Writing: C.S., H.L.A., S.G.W.; Supervision: H.L.A., S.G.W.; Funding Acquisition: H.L.A.

## References

Applewhite DA, Barzik M, Kojima S, Svitkina TM, Gertler FB, Borisy GG. 2007. Ena/VASP proteins have an anti-capping independent function in filopodia formation. *Mol Biol Cell* **18**: 2579-2591.

Barzik M, Kotova TI, Higgs HN, Hazelwood L, Hanein D, Gertler FB, Schafer DA. 2005. Ena/VASP proteins enhance actin polymerization in the presence of barbed end capping proteins. *J Biol Chem* **280**: 28653-28662.

Bear JE, Loureiro JJ, Libova I, Fassler R, Wehland J, Gertler FB. 2000. Negative regulation of fibroblast motility by Ena/VASP proteins. *Cell* **101**: 717-728.

Bear JE, Svitkina TM, Krause M, Schafer DA, Loureiro JJ, Strasser GA, Maly IV, Chaga OY, Cooper JA, Borisy GG et al. 2002. Antagonism between Ena/VASP proteins and actin filament capping regulates fibroblast motility. *Cell* **109**: 509-521.

Breitsprecher D, Kiesewetter AK, Linkner J, Urbanke C, Resch GP, Small JV, Faix J. 2008. Clustering of VASP actively drives processive, WH2 domain-mediated actin filament elongation. *EMBO J* **27**: 2943-2954.

Caldwell AB, Liu Q, Schroth GP, Galasko DR, Yuan SH, Wagner SL, Subramaniam S. 2020. Dedifferentiation and neuronal repression define familial Alzheimer's disease. *Sci Adv* **6**.

Chanet S, Huynh JR. 2020. Collective Cell Sorting Requires Contractile Cortical Waves in Germline Cells. *Curr Biol* **30**: 4213-4226 e4214.

Chen D, McKearin D. 2003. Dpp signaling silences bam transcription directly to establish asymmetric divisions of germline stem cells. *Curr Biol* **13**: 1786-1791.

Daly CA, Hall ET, Ogden SK. 2022. Regulatory mechanisms of cytoneme-based morphogen transport. *Cell Mol Life Sci* **79**: 119.

de Cuevas M, Spradling AC. 1998. Morphogenesis of the Drosophila fusome and its implications for oocyte specification. *Development* **125**: 2781-2789.

Gates J, Mahaffey JP, Rogers SL, Emerson M, Rogers EM, Sottile SL, Van Vactor D, Gertler FB, Peifer M. 2007. Enabled plays key roles in embryonic epithelial morphogenesis in Drosophila. *Development* **134**: 2027-2039.

Gates J, Nowotarski SH, Yin H, Mahaffey JP, Bridges T, Herrera C, Homem CC, Janody F, Montell DJ, Peifer M. 2009. Enabled and Capping protein play important roles in shaping cell behavior during Drosophila oogenesis. *Dev Biol* **333**: 90-107.

Gertler FB, Niebuhr K, Reinhard M, Wehland J, Soriano P. 1996. Mena, a relative of VASP and Drosophila Enabled, is implicated in the control of microfilament dynamics. *Cell* **87**: 227-239.

Guo Y, Wu W, Yang X, Fu X. 2022. Dedifferentiation and in vivo reprogramming of committed cells in wound repair (Review). *Mol Med Rep* **26**.

Homem CC, Peifer M. 2009. Exploring the roles of diaphanous and enabled activity in shaping the balance between filopodia and lamellipodia. *Mol Biol Cell* **20**: 5138-5155.

Kai T, Spradling A. 2003. An empty Drosophila stem cell niche reactivates the proliferation of ectopic cells. *Proc Natl Acad Sci U S A* **100**: 4633-4638.

-. 2004. Differentiating germ cells can revert into functional stem cells in Drosophila melanogaster ovaries. *Nature* **428**: 564-569.

Kang F, Laine RO, Bubb MR, Southwick FS, Purich DL. 1997. Profilin interacts with the Gly-Pro-Pro-Pro-Pro-Pro sequences of vasodilator-stimulated phosphoprotein

(VASP): implications for actin-based Listeria motility. *Biochemistry* **36**: 8384-8392.

Kirilly D, Xie T. 2007. The Drosophila ovary: an active stem cell community. *Cell Res* **17**: 15-25.

Lebrand C, Dent EW, Strasser GA, Lanier LM, Krause M, Svitkina TM, Borisy GG, Gertler FB. 2004. Critical role of Ena/VASP proteins for filopodia formation in neurons and in function downstream of netrin-1. *Neuron* **42**: 37-49.

Lin H, Yue L, Spradling AC. 1994. The Drosophila fusome, a germline-specific organelle, contains membrane skeletal proteins and functions in cyst formation. *Development* **120**: 947-956.

Liu Z, Zhong G, Chai PC, Luo L, Liu S, Yang Y, Baeg GH, Cai Y. 2015. Coordinated niche-associated signals promote germline homeostasis in the Drosophila ovary. *J Cell Biol* **211**: 469-484.

McKearin D, Ohlstein B. 1995. A role for the Drosophila bag-of-marbles protein in the differentiation of cystoblasts from germline stem cells. *Development* **121**: 2937-2947.

McKearin DM, Spradling AC. 1990. bag-of-marbles: a Drosophila gene required to initiate both male and female gametogenesis. *Genes Dev* **4**: 2242-2251.

Mejillano MR, Kojima S, Applewhite DA, Gertler FB, Svitkina TM, Borisy GG. 2004. Lamellipodial versus filopodial mode of the actin nanomachinery: pivotal role of the filament barbed end. *Cell* **118**: 363-373.

Nichols JM, Antolovic V, Reich JD, Brameyer S, Paschke P, Chubb JR. 2020. Cell and molecular transitions during efficient dedifferentiation. *Elife* **9**.

Niebuhr K, Ebel F, Frank R, Reinhard M, Domann E, Carl UD, Walter U, Gertler FB, Wehland J, Chakraborty T. 1997. A novel proline-rich motif present in ActA of Listeria monocytogenes and cytoskeletal proteins is the ligand for the EVH1 domain, a protein module present in the Ena/VASP family. *EMBO J* **16**: 5433-5444.

Nowotarski SH, McKeon N, Moser RJ, Peifer M. 2014. The actin regulators Enabled and Diaphanous direct distinct protrusive behaviors in different tissues during Drosophila development. *Mol Biol Cell* **25**: 3147-3165.

Ohlstein B, McKearin D. 1997. Ectopic expression of the Drosophila Bam protein eliminates oogenic germline stem cells. *Development* **124**: 3651-3662.

Pasic L, Kotova T, Schafer DA. 2008. Ena/VASP proteins capture actin filament barbed ends. *J Biol Chem* **283**: 9814-9819.

Ramirez-Weber FA, Kornberg TB. 1999. Cytonemes: cellular processes that project to the principal signaling center in Drosophila imaginal discs. *Cell* **97**: 599-607.

Reinhard M, Giehl K, Abel K, Haffner C, Jarchau T, Hoppe V, Jockusch BM, Walter U. 1995. The proline-rich focal adhesion and microfilament protein VASP is a ligand for profilins. *EMBO J* **14**: 1583-1589.

Rogers S, Zhang C, Anagnostidis V, Liddle C, Fishel ML, Gielen F, Scholpp S. 2023. Cancer-associated fibroblasts influence Wnt/PCP signaling in gastric cancer cells by cytoneme-based dissemination of ROR2. *Proc Natl Acad Sci U S A* **120**: e2217612120.

Rojas-Rios P, Guerrero I, Gonzalez-Reyes A. 2012. Cytoneme-mediated delivery of hedgehog regulates the expression of bone morphogenetic proteins to maintain germline stem cells in Drosophila. *PLoS Biol* **10**: e1001298.

Rottner K, Behrendt B, Small JV, Wehland J. 1999. VASP dynamics during lamellipodia protrusion. *Nat Cell Biol* **1**: 321-322.

Samuels TJ, Gui J, Gebert D, Karam Teixeira F. 2024. Two distinct waves of transcriptome and translatome changes drive Drosophila germline stem cell differentiation. *EMBO J* **43**: 1591-1617.

Sano H, Kunwar PS, Renault AD, Barbosa V, Clark IB, Ishihara S, Sugimura K, Lehmann R. 2012. The Drosophila actin regulator ENABLED regulates cell shape and orientation during gonad morphogenesis. *PLoS One* **7**: e52649.

Schindelin J, Arganda-Carreras I, Frise E, Kaynig V, Longair M, Pietzsch T, Preibisch S, Rueden C, Saalfeld S, Schmid B et al. 2012. Fiji: an open-source platform for biological-image analysis. *Nat Methods* **9**: 676-682.

Schirenbeck A, Arasada R, Bretschneider T, Stradal TE, Schleicher M, Faix J. 2006. The bundling activity of vasodilator-stimulated phosphoprotein is required for filopodium formation. *Proc Natl Acad Sci U S A* **103**: 7694-7699.

Schwitalla S, Fingerle AA, Cammareri P, Nebelsiek T, Goktuna SI, Ziegler PK, Canli O, Heijmans J, Huels DJ, Moreaux G et al. 2013. Intestinal tumorigenesis initiated by dedifferentiation and acquisition of stem-cell-like properties. *Cell* **152**: 25-38.

Scott JA, Shewan AM, den Elzen NR, Loureiro JJ, Gertler FB, Yap AS. 2006. Ena/VASP proteins can regulate distinct modes of actin organization at cadherin-adhesive contacts. *Mol Biol Cell* **17**: 1085-1095.

Sheng XR, Brawley CM, Matunis EL. 2009. Dedifferentiating spermatogonia outcompete somatic stem cells for niche occupancy in the Drosophila testis. *Cell Stem Cell* **5**: 191-203.

Song X, Wong MD, Kawase E, Xi R, Ding BC, McCarthy JJ, Xie T. 2004. Bmp signals from niche cells directly repress transcription of a differentiation-promoting gene, bag of marbles, in germline stem cells in the Drosophila ovary. *Development* **131**: 1353-1364.

Song X, Zhu CH, Doan C, Xie T. 2002. Germline stem cells anchored by adherens junctions in the Drosophila ovary niches. *Science* **296**: 1855-1857.

Sutcliffe B, Ng J, Auer TO, Pasche M, Benton R, Jefferis GS, Cachero S. 2017. Second-Generation Drosophila Chemical Tags: Sensitivity, Versatility, and Speed. *Genetics* **205**: 1399-1408.

Svitkina TM, Bulanova EA, Chaga OY, Vignjevic DM, Kojima S, Vasiliev JM, Borisy GG. 2003. Mechanism of filopodia initiation by reorganization of a dendritic network. *J Cell Biol* **160**: 409-421.

Takahashi K, Yamanaka S. 2016. A decade of transcription factor-mediated reprogramming to pluripotency. *Nat Rev Mol Cell Biol* **17**: 183-193.

Wilcockson SG, Ashe HL. 2019. Drosophila Ovarian Germline Stem Cell Cytocensor Projections Dynamically Receive and Attenuate BMP Signaling. *Dev Cell* **50**: 296-312 e295.

-. 2021. Live imaging of the Drosophila ovarian germline stem cell niche. *STAR Protoc* **2**: 100371.

Winkelman JD, Bilancia CG, Peifer M, Kovar DR. 2014. Ena/VASP Enabled is a highly processive actin polymerase tailored to self-assemble parallel-bundled F-actin networks with Fascin. *Proc Natl Acad Sci U S A* **111**: 4121-4126.

Xie T, Spradling AC. 1998. decapentaplegic is essential for the maintenance and division of germline stem cells in the Drosophila ovary. *Cell* **94**: 251-260.

-. 2000. A niche maintaining germ line stem cells in the Drosophila ovary. *Science* **290**: 328-330.

Sutcliffe_Fig_1

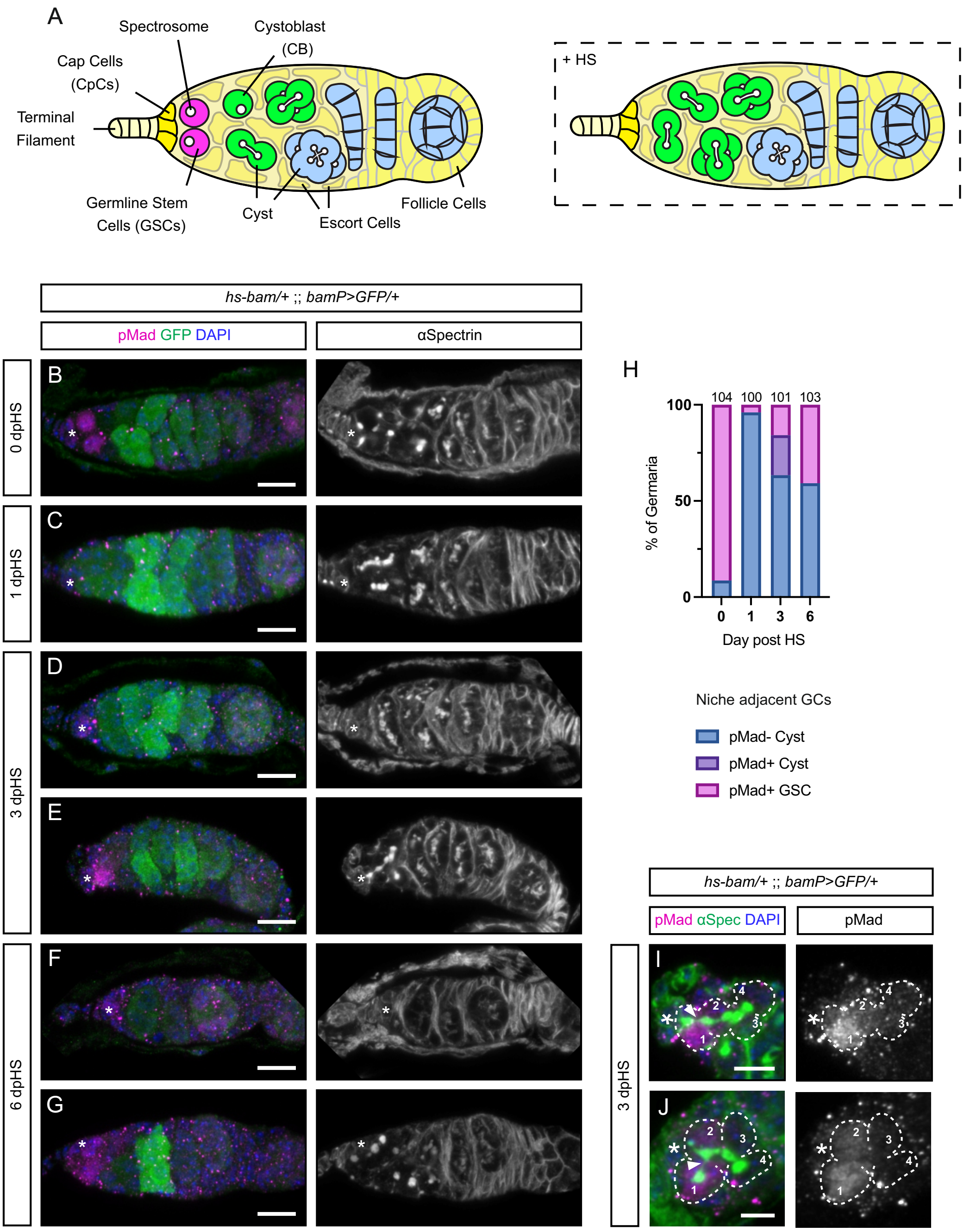
A
Spectrosome
Cystoblast
(CB)
Cap Cells
(CpCs)
Terminal
Filament
Germline Stem
Cells (GSCs)
Cyst
Escort Cells
Follicle Cells
+ HS
hs-bam/+ ;; bamP>GFP/+
pMad GFP DAPI
αSpectrin
B
C
D
E
F
G
0 dpHS
1 dpHS
3 dpHS
6 dpHS
*
H
104
100
101
103
100
50
0
% of Germaria
0
1
3
6
Day post HS
Niche adjacent GCs
pMad- Cyst
pMad+ Cyst
pMad+ GSC
hs-bam/+ ;; bamP>GFP/+
pMad αSpec DAPI
pMad
I
J
3 dpHS
1
2
3
4

**Figure 1: GCs dedifferentiate over time to reoccupy the niche**

(A) Schematic of the germarium with the different cell types, as labelled, anterior is to the left. The spectrosome and fusomes are shown in white. The boxed germarium shows post-heatshock induced *bam* expression.

(B-E) Germaria carrying *bam* promoter-GFP and *hs-bam* transgenes immunostained with anti-pMad (magenta), anti-GFP (green) and anti-αSpectrin (grey, right panel). Representative germaria are shown for day 0 (B) and post-HS at day 1 (C), 3 (D-E) and 6 (F-G). (*) Cap cells. Scale bar, 10μm.

(H) Quantitation of the number of germaria where the GCs contacting the niche are pMad positive or negative differentiating cysts or pMad positive GSCs on days 0, 1, 3 and 6 post-HS. The number of germaria counted per time point is indicated above the graph.

(I and J) pMad positive cysts on day 3 post-HS with pMad staining shown as a single channel (grey). Connected CBs are outlined and numbered 1 to 4 in the 4-cell cyst. (*) Cap cells, arrowhead shows a fusome undergoing scission. Scale bar, 5μm.

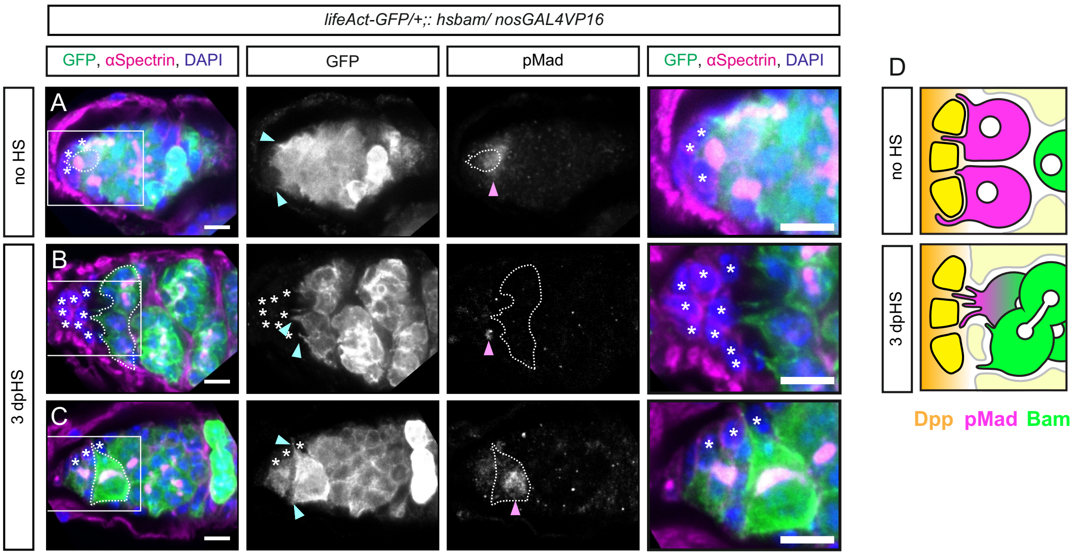
lifeAct-GFP/+;: hsbam/ nosGAL4VP16
GFP, αSpectrin, DAPI
GFP
pMad
GFP, αSpectrin, DAPI
A
B
C
D
no HS
3 dpHS
no HS
3 dpHS
Dpp pMad Bam

**Figure 2: Dedifferentiating GCs extend cytonemes during niche recolonisation**
(A-C) Germaria carrying *lifeAct-GFP* driven by *nosGAL4VP16* and a *hs-bam* transgene immunostained with anti-GFP (green and inset), anti-αSpectrin (magenta) and anti-pMad (inset). non-HS control (A), 3 dpHS germaria (B-C) with (B) a pMad negative 8-cell cyst extending cytonemes to the niche and (C) a pMad positive GSC with cytonemes contacting the niche. (*) Niche cells including extra somatic cells, cyan arrowheads mark cytonemes, magenta arrowheads indicate pMad positive cells. Scale Bar, 5µm.
(D) Schematic of the germarium niche showing no HS GSCs and a 3 dpHS cyst which extends cytonemes toward the niche and is BMP responsive.

Sutcliffe_Fig_3

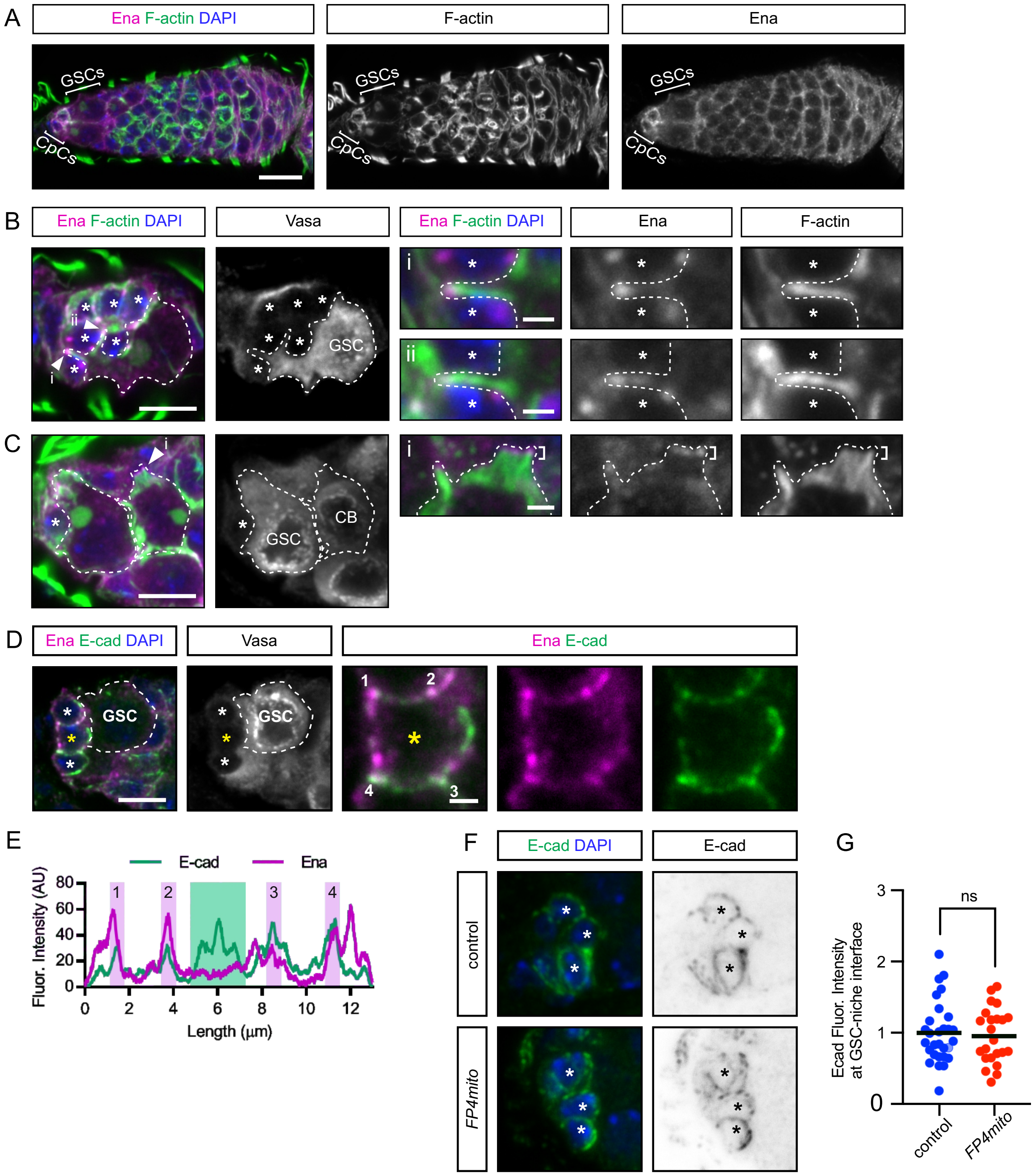
A
Ena F-actin DAPI
F-actin
Ena
GSCs
CpCs
B
Ena F-actin DAPI
Vasa
Ena F-actin DAPI
Ena
F-actin
GSC
i
ii
C
CB
GSC
D
Ena E-cad DAPI
Vasa
Ena E-cad
GSC
1
2
3
4
E
E-cad
Ena
Fluor. Intensity (AU)
0
20
40
60
80
0
2
4
6
8
10
12
Length (µm)
F
E-cad DAPI
E-cad
control
FP4mito
G
Ecad Fluor. Intensity at GSC-niche interface
ns
0
1
2
3
control
FP4mito

**Figure 3: Ena is localised to cytoneme tips**

(A) Wildtype germarium immunostained with anti-Ena (magenta) and Phalloidin (green). GSCs and CpCs are marked by brackets. Scale bar, 10µm.

(B) Immunostaining as in (A) and Vasa (grey inset). A GSC is outlined by a dotted line, white arrowheads mark cytonemes (i and ii), that are shown as higher magnification images. (*) Cap Cells. Scale bar, 5µm and (i-ii) 1µm.

(C) Immunostaining as in (B). A GSC and CB are outlined by dotted lines. A CB cytoneme is indicated by a white arrowhead and shown magnified in (i). Lamellipodial projections are indicated by brackets. (*) Cap Cells. Scale bar, 5µm and (i) 1µm.

(D) Wildtype germarium immunostained with anti-Ena (magenta) and anti-Ecad (green). GSC is outlined by a dotted line. (*) Cap Cells. Scale bar, 5µm.

(E) Intensity plot for Ena and eCadherin staining shown in (D) across points 1-4 of CpC marked with a yellow (*)

(F) Control and *FP4mito* expressing germaria immunostained with anti-Ecad (green and grey inset).

(G) Intensity plot for Ecad staining shown in (F), n=29 and 23, Welch's unpaired two-tailed t test, p =0.5942 (ns)

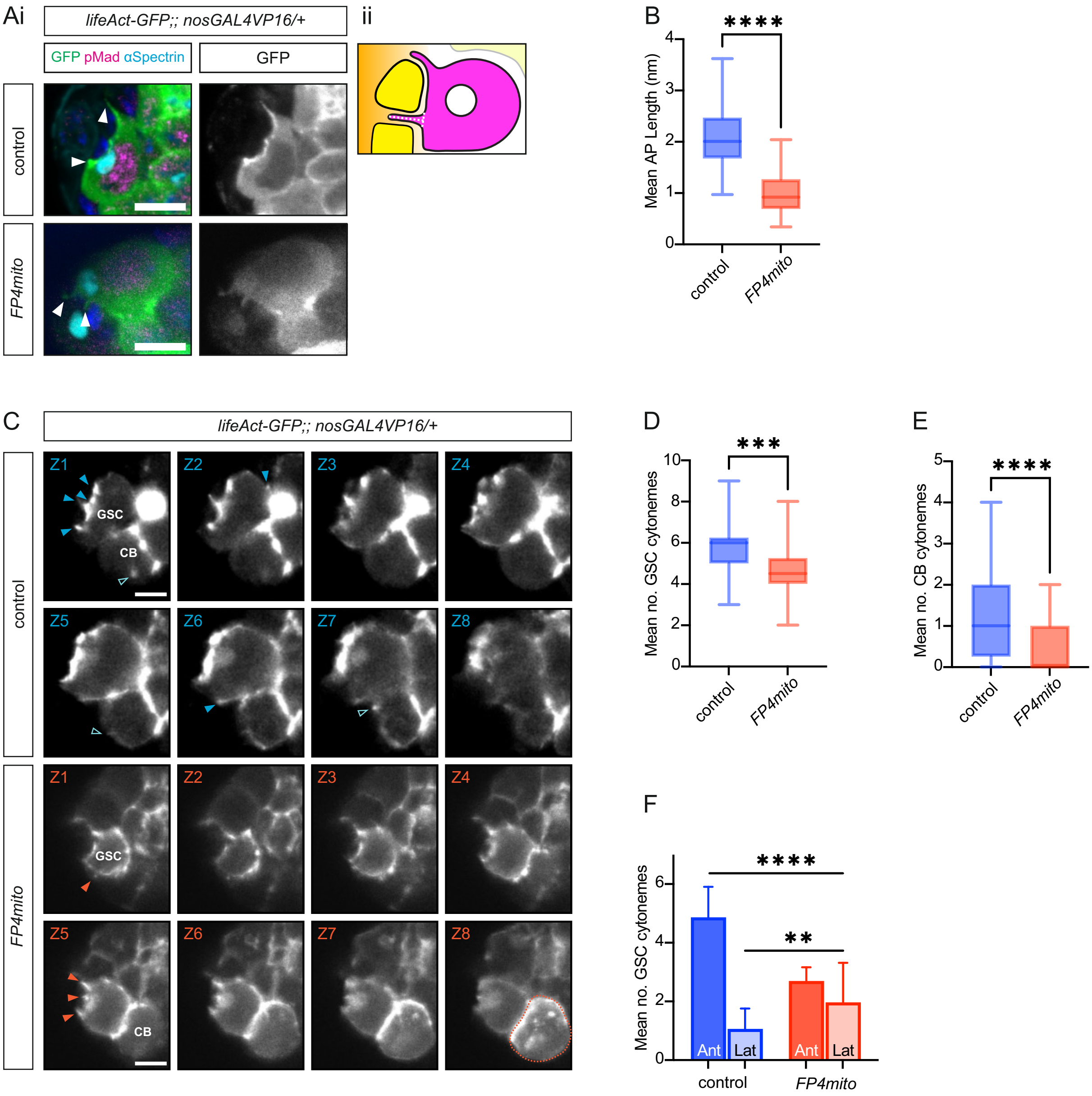
Ai
lifeAct-GFP;; nosGAL4VP16/+
GFP pMad αSpectrin
GFP
control
FP4mito
ii
B
****
Mean AP Length (nm)
0
1
2
3
4
control
FP4mito
C
lifeAct-GFP;; nosGAL4VP16/+
control
FP4mito
Z1
Z2
Z3
Z4
Z5
Z6
Z7
Z8
GSC
CB
D
***
Mean no. GSC cytonemes
0
2
4
6
8
10
control
FP4mito
E
****
Mean no. CB cytonemes
0
1
2
3
4
5
control
FP4mito
F
****
**
Mean no. GSC cytonemes
0
2
4
6
Ant
Lat
Ant
Lat
control
FP4mito

**Figure 4: Ena regulates GC cytoneme formation**

(A) Germaria expressing *lifeAct-GFP* driven by *nosGAL4VP16*, which are either control or carry a *FP4mito* transgene. Immunostaining with anti-GFP (green and grey inset), anti-pMad (magenta), anti-αSpectrin (cyan) and DAPI (blue). (i) Schematic of a GSC with the length measurement shown for one cytoneme (dotted white line). (*) Cap Cells. Scale bar, 5μm.

(B) Graph shows the lengths of GSC cytonemes from fixed control and FP4mito germaria, as shown in (A) for representative examples. n = 36 cytonemes, Welch's unpaired t test, p = <0.0001.

(C) Single time point Z-series from a live imaging movie of control or FP4mito germaria carrying *lifeActin-GFP* driven by *nosGAL4VP16*. Each panel shows a single Z-slice (Z1-8). Closed and open arrowheads indicate GSC and CB cytonemes, respectively. Scale bar, 10μm.

(D, E) Graphs show the mean number of GSC and CB cytonemes from live imaging movies, a still from a representative movie is shown in (C). n = 15, across 36 time points. Welch’s unpaired t test, $p = 0.0005$ (D) and $p = <0.0001$ (E).

(F) As in (D) except the graphs shows the mean number of anteriorly or laterally oriented GSC cytonemes. n = 15, across 36 time points. Welch’s t test, $p = <0.0001$ and $p = 0.0023$ for comparisons between genotypes of the number of anterior and lateral cytonemes, respectively.

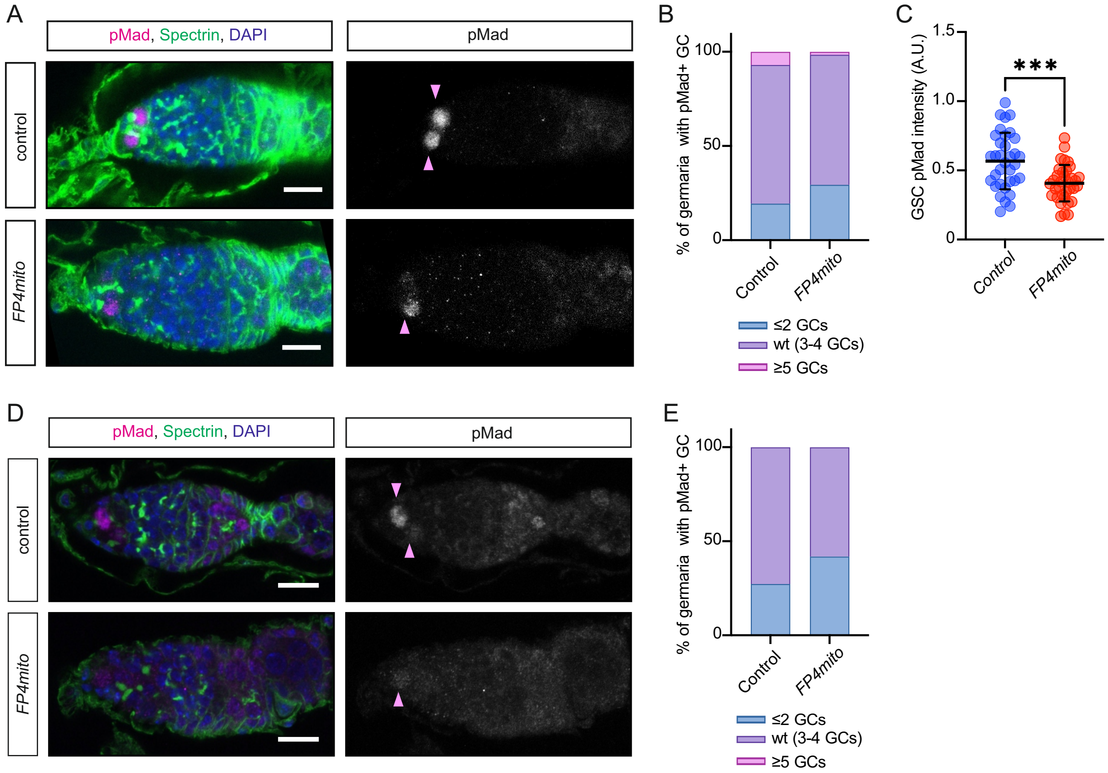
A
pMad, Spectrin, DAPI
pMad
control
FP4mito
B
% of germaria with pMad+ GC
100
50
0
Control
FP4mito
≤2 GCs
wt (3-4 GCs)
≥5 GCs
C
GSC pMad intensity (A.U.)
1.5
1.0
0.5
0
***
Control
FP4mito
D
pMad, Spectrin, DAPI
pMad
control
FP4mito
E
% of germaria with pMad+ GC
100
50
0
Control
FP4mito
≤2 GCs
wt (3-4 GCs)
≥5 GCs

**Figure 5: Ena mislocalisation impairs BMP signal reception and stem cell fitness**
(A) Representative images of control or *FP4mito* germaria aged for 7 days, immunostained with anti-pMad (magenta and single channel), anti-αSpectrin (green) and DAPI (blue). Magenta arrowheads indicate pMad positive GCs. Scale bar, 10µm.
(B) Graph shows the number of pMad positive GCs counted in 7 day old germaria including the representative germaria shown in (A), n >100.
(C) Graph shows the pMad intensity in GSCs in control and *FP4mito* backgrounds, including the representative germaria shown in (B). n = 34 per genotype. Welch's t two-tailed unpaired t- test, p = 0.0003 for comparisons between genotypes.
(D) Germaria aged for 2.5 weeks carrying *lifeActin-GFP* driven by *nosGAL4VP16*, which are either control or carry a *FP4mito* transgene. Immunostaining with anti-αSpectrin (green), anti-pMad (magenta and inset) and DAPI (blue). Magenta arrowheads indicate pMad positive GCs. Scale bar 10µm.
(E) Graph shows the number of pMad positive GCs counted in 2.5-week-old germaria from (D). n = 50

Sutcliffe_Fig_6

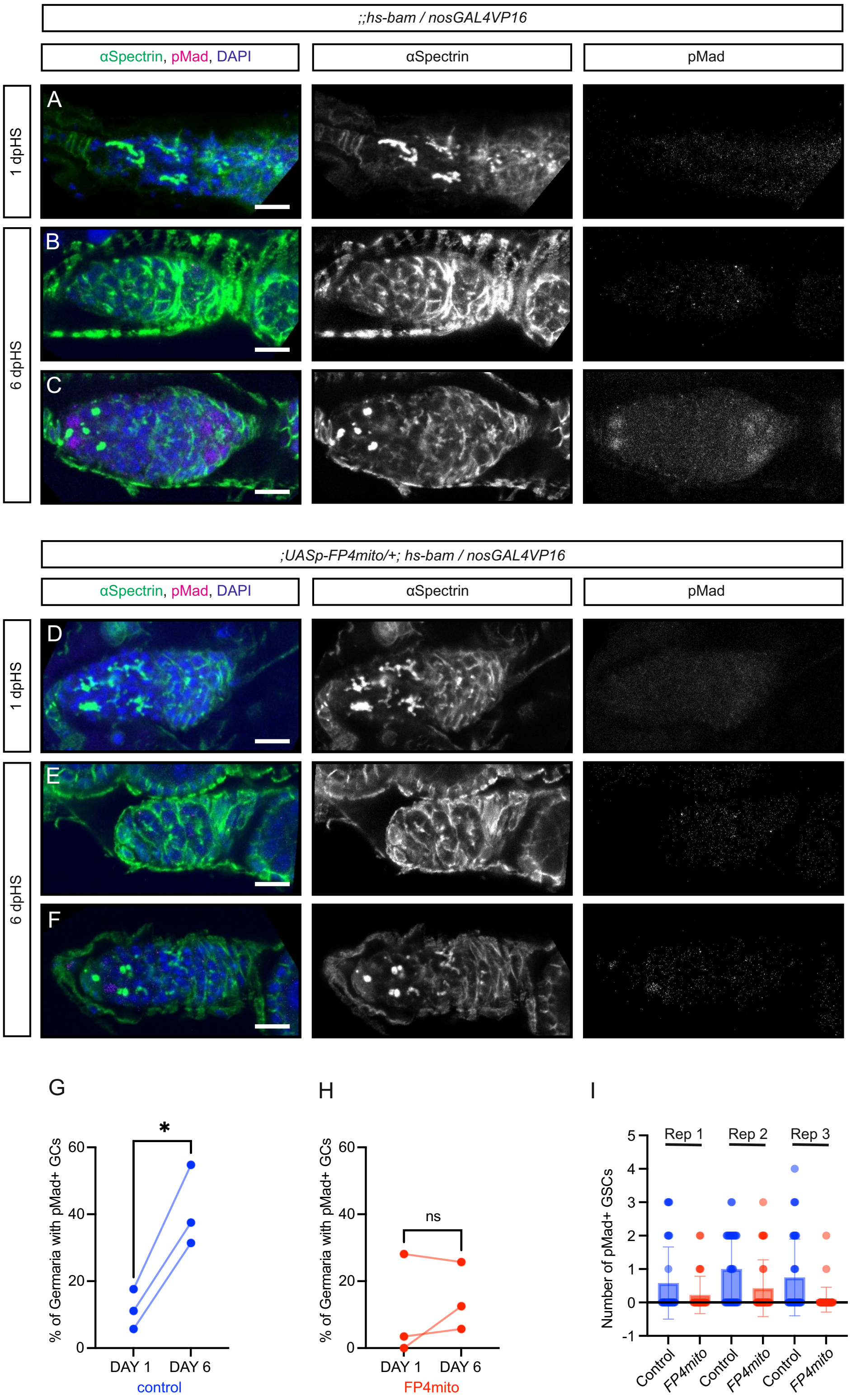
;;hs-bam / nosGAL4VP16
αSpectrin, pMad, DAPI
αSpectrin
pMad
1 dpHS
6 dpHS
A
B
C
;UASp-FP4mito/+; hs-bam / nosGAL4VP16
αSpectrin, pMad, DAPI
αSpectrin
pMad
1 dpHS
6 dpHS
D
E
F
G
% of Germaria with pMad+ GCs
0
20
40
60
*
DAY 1
DAY 6
control
H
% of Germaria with pMad+ GCs
0
20
40
60
ns
DAY 1
DAY 6
FP4mito
I
Number of pMad+ GSCs
-1
0
1
2
3
4
5
Rep 1
Rep 2
Rep 3
Control
FP4mito
Control
FP4mito
Control
FP4mito

**Figure 6: Ena mislocalisation impairs GSC dedifferentiation**

(A-C) Control germaria carrying a *hs-bam* transgene and *nosGAL4VP16* immunostained with anti-pMad (magenta and inset) and anti-ɑSpectrin (green and inset). Representative germaria are shown for day 1 (A) and 6 (B-C) post heat shock. Scale bar; 10μm.

(D-F) As in (A-C), except germaria also carry a *UASp-FP4mito-halo7* transgene. Scale bar; 10μm.

(G, H) Quantification of germaria containing pMad positive early GCs on day 1 and day 6 post-HS for (G) control and (H) *FP4mito*. Data are pairwise comparisons, two-tailed paired t test comparing day 1 to day 6, $p = 0.0150$ for control (*) and $p= 0.448$ for FP4mito (ns). Each repeat contains at least 30 germaria.

(I) Quantification of the number of pMad positive GSCs per germaria for each repeat.

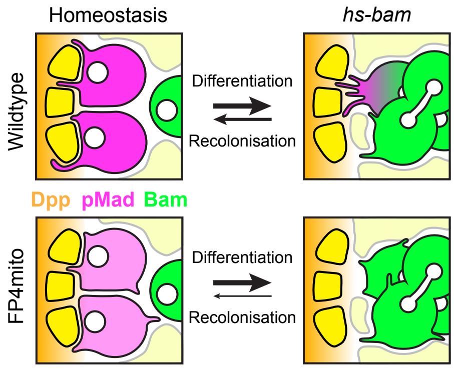
Homeostasis
*hs-bam*
Wildtype
Differentiation
Recolonisation
Dpp
pMad
Bam
FP4mito
Differentiation
Recolonisation

**Figure 7: Cytonemes promote stem cell fitness and enable cyst dedifferentation**
Model of the role of cytonemes in the ovarian germline at homeostasis, in promoting Dpp signalling and stem cell fitness, and in dedifferentiation, by enabling cysts to access niche-derived Dpp.